Two polarization-entangled sources from the same semiconductor chip

Dongpeng Kang,* Minseok Kim, Haoyu He, and Amr S. Helmy
The Edward S. Rogers Department of Electrical and Computer Engineering, Centre for Quantum Information and Quantum Control, University of Toronto, 10 King's College Road, Toronto, Ontario, Canada M5S 3G4
(Received 6 December 2014; published 13 July 2015)

Generating nonclassical states of photons such as polarization-entangled states on a monolithic chip is a crucial step towards practical applications of optical quantum information processing such as quantum computing and quantum key distribution. Here we demonstrate two polarization-entangled photon sources in a single monolithic semiconductor waveguide. The first source is achieved through the concurrent utilization of two spontaneous parametric down-conversion (SPDC) processes, namely, type-0 and type-I SPDC processes. The chip can also generate polarization-entangled photons via the type-II SPDC process, enabling the generation of both copolarized- and cross-polarized polarization-entangled photons in the same device. In both cases, polarization entanglement is generated directly on the chip without the use of any off-chip compensation, interferometry, or bandpass filtering. This enables direct, chip-based generation of both Bell states $(|H,H\rangle + |V,V\rangle)/\sqrt{2}$ and $(|H,V\rangle + |V,H\rangle)/\sqrt{2}$ simultaneously utilizing the same pump source. In addition, based on compound semiconductors, this chip can be directly integrated with it own pump laser. This technique ushers an era of self-contained, integrated, electrically pumped, room-temperature polarization-entangled photon sources.

DOI: 10.1103/PhysRevA.92.013821 PACS number(s): 42.65.Lm, 42.50.Dv, 03.67.Bg, 42.82.Et

I. INTRODUCTION

Entangled photons are essential building blocks for optical quantum information processing, such as quantum computing (QC) [1] and quantum key distribution (QKD) [2]. Conventionally, entangled photons have been generated using a myriad of techniques, most notably by using the process of spontaneous parametric down-conversion (SPDC) utilizing second-order nonlinearities in crystals [3]. Properties such as brightness, scalability, compact form factors, and room-temperature operation play key roles in enabling us to fully profit from entangled photon sources in applications such as QC and QKD. As such, the physics and technology of generating and manipulating entangled photons in monolithic settings have recently been topics of immense interest. Harnessing such effects in a monolithic form factor also enables further incorporation of other photonic components that may be necessary for the aforementioned applications [4–7]. This provided the drive that motivated the early work on implementing entangled sources in waveguides of crystals with appreciable second-order nonlinearities such as lithium niobate [8].

Realizing entangled photon sources in monolithic settings enables much more than the inclusion of numerous necessary components simultaneously: It can enable the direct generation of novel and useful photonic quantum states with specified properties, without moving parts, while benefiting from the accurate alignment of nanolithography, precision of epitaxial growth, and thin-film deposition techniques. For example, monolithic platforms offer opportunities to provide photons that are entangled in one or several degrees of freedom simultaneously without the need for any extra component on the chip [9,10]. In addition, monolithic sources can offer significant control over the spectral-temporal properties of the entangled photons with relative ease and high precision [11]. This in turn provides a powerful tool for tailoring the temporal correlation or the spectral bandwidth of the photon states. Such states can be of extremely short correlation times, which can enhance the accuracy of protocols for quantum positioning and timing [12] and the sensitivity offered by quantum illumination [13]. The same integrated sources can generate states with extremely large temporal correlation times. This in turn leads to narrow spectral bandwidth, which can provide a more efficient atom-photon interface and improved sources for long-haul QKD [14].

The vast majority of the aforementioned applications use polarization-entangled photon sources. Entanglement in the polarization degree of freedom has been the most widely utilized to implement entangled sources for experiments and applications that probe or exploit quantum effects. Photon pairs in polarization-entangled sources need to be indistinguishable in every degree of freedom, except for polarization, which is challenging to achieve for states produced directly in waveguides [8,15,16]. For photon pairs generated in a type-II process, in which the down-converted photons are cross polarized, the birefringence in the group velocities of the modes, where the photons propagate, will cause a temporal walkoff between the pair, allowing polarization to be inferred from the photon arrival time. On the other hand, for photon pairs generated in a type-0 or type-I process, where the photons in a pair are copolarized, there is a lack of two orthogonal polarizations necessary for polarization entanglement. As a result, most waveguide sources of photon pairs require an off-chip compensation setup [15] or an interferometer [16] to generate polarization entanglement, which increases the source complexity and decreases the system stability significantly.

Recently, several techniques have been demonstrated to generate polarization-entangled photons from a monolithic chip [17–20]. The approaches that use spontaneous four-wave mixing in Si-based chips utilize integrated photonic components such as on-chip polarization rotators [17] or two-dimensional grating couplers [18] and benefit from mature fabrication technologies. However, the indirect band gap of

*dongpeng.kang@mail.utoronto.ca

Si presents significant challenges for further integration with the pump lasers. To this end, III–V semiconductor material systems offer an optimal solution in terms of functionality to tailor the dispersion and birefringence as well as monolithic integration with the pump lasers [21,22]. Techniques using the counterpropagating phase-matching (PM) scheme [19] and modal PM in Bragg reflection waveguides (BRWs) [20] based on AlGaAs have been demonstrated. In the former case, however, the requirement of two pump beams with strictly controlled incidence angles and beam shapes imposes a significant challenge for further integration, while in the latter case, the spectral distinguishability and walkoff due to modal birefringence compromise the quality of entanglement.

In this work, we demonstrate how the waveguiding physics associated with BRWs can be used to simultaneously produce two polarization-entangled photon sources using alternative approaches in a single self-contained room-temperature semiconductor chip. The waveguide structure utilized is schematically shown in Fig. 1(a). The chip, based on a single monolithic semiconductor BRW, is straightforward to design and implement and has no moving parts. The technique allows direct polarization-entanglement generation using an extremely simple setup without any off-chip walkoff compensation, interferometer, or even bandpass filtering. The first source is achieved through the concurrent utilization of two second-order processes, namely, type-0 and type-I SPDC processes, pumped by a single waveguide mode [23] as opposed to two modes of different polarizations [17] or modes propagating in opposite directions [19]. This approach permits the integration of the pump with the source in a monolithic form. Within the same waveguide, there exists a second source based on a type-II process due to the lack of material birefringence [20]. The virtual energy diagrams of the two sources are also schematically shown in Fig. 1(a). As such, in this approach, by varying the pump polarization and wavelength, one can select between both polarization-entangled sources or use them concomitantly. The direct generation of both Bell states $(|H,H\rangle + |V,V\rangle)/\sqrt{2}$ and $(|H,V\rangle + |V,H\rangle)/\sqrt{2}$ on a single chip can be envisaged. In addition, by lithographically tuning the waveguide ridge width, one can tune the degree of entanglement of the first source.

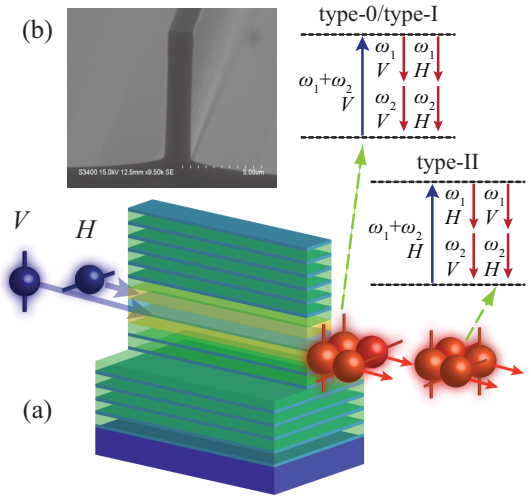

FIG. 1. (Color online) (a) Schematic of the multilayer BRWs as sources of polarization-entangled photons. Entangled photons can be generated via concurrent type-0 and type-I processes, in which a TM-polarized pump photon generates a pair of copolarized photons, either both TE or both TM polarized. Instead, entangled photons can also be produced via the type-II process, in which a TE pump photon produces a pair of cross-polarized photons. Paired photons will be spatially separated, in this case, by a beam splitter. The virtual energy diagrams of the two possible decaying channels for both entanglement generation mechanisms are also plotted. (b) A scanning electron microscope image of the fabricated waveguide.

II. METHODS

For concurrent type-0 and type-I processes with a shared TM-polarized pump, paired photons can be generated either in TM polarizations via the type-0 process or in TE polarizations via the type-I process. In the ideal case, photon pairs can be produced from the two processes with the same efficiency and identical spectrum, which renders them in a maximally entangled state $[|H,H\rangle + \exp(i\phi)|V,V\rangle]/\sqrt{2}$. This is the approach that we pursue to obtain a chip-based entangled source using the type-0 and type-I interactions.

The AlGaAs structure used to demonstrate these sources was grown on a [001] GaAs substrate and the waveguide direction was oriented along [110]. Due to the zinc-blende crystal symmetry, the nonlinear tensor $\chi^{(2)}_{ijk}$ is nonzero only when $i \neq j \neq k$, with $i,j,k = x,y,x$ being the crystal coordinates. As a result, three SPDC processes, namely, type-0, type-I, and type-II processes, could coexist provided PM is satisfied. Among them, the type-0 process depends on the electric-field components of the interacting modes along the propagation direction, which are usually negligible in weakly guided waveguides. In BRWs, however, due to the index variations between different layers, the efficiency of the type-0 process can be significant and can even be markedly tuned by engineering the epitaxial structure [23]. In order to achieve concurrent PM of type-0 and type-I processes, the effective indices of the pump $n_{\mathrm{TM}}(2\omega)$ should be equal to those of the down-converted photons $n_{\mathrm{TE}}(\omega)$ and $n_{\mathrm{TM}}(\omega)$ simultaneously, i.e., $n_{\mathrm{TM}}(2\omega) = n_{\mathrm{TE}}(\omega) = n_{\mathrm{TM}}(\omega)$, with ω indicating the degenerate PM frequency of the down-converted photons and TE and TM indicating the polarizations. This requirement can be satisfied lithographically by tuning the ridge width.

The two-photon state generated via the two concurrent SPDC processes is given by [10,24]

$$|\psi\rangle = \frac{1}{\sqrt{\eta_{\mathrm{I}} + \eta_0}} \iint d\omega_1 d\omega_2 [\sqrt{\eta_{\mathrm{I}}}\Phi_{HH}(\omega_1,\omega_2)|H\omega_1, H\omega_2\rangle + \sqrt{\eta_0}\Phi_{VV}(\omega_1,\omega_2)|V\omega_1, V\omega_2\rangle], \quad (1)$$

where η_{I} and η_0 are the generation rates (pairs per pump photon) of the two processes after taking into account the losses and $\Phi_{HH}(\omega_1,\omega_2)$ and $\Phi_{VV}(\omega_1,\omega_2)$ are the biphoton wave functions, with the subscripts indicating the photon polarizations, and satisfy the normalization condition $\iint d\omega_1 d\omega_2 |\Phi_{HH(VV)}(\omega_1,\omega_2)|^2 = 1$. When spatially separated, the paired photons are polarization entangled. The two spectra are found to be almost identical, as shown in Fig. 2(a).

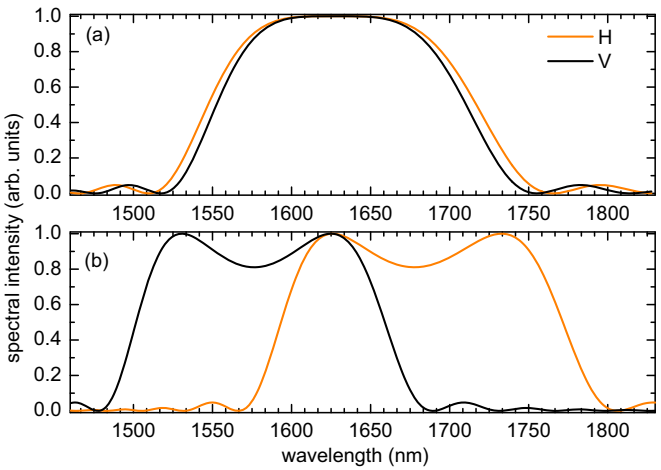

FIG. 2. (Color online) Simulated spectral intensities of (a) H- and V-polarized photons generated via the type-I and type-0 processes, respectively, and (b) photons generated via the type-II process. The waveguide length is assumed to be 1.05 mm, the same as the waveguide tested in the experiment.

As a result, Eq. (1) is maximally entangled when the generation rates are the same, i.e., $\eta_I = \eta_0$. In this case, there is no way, even in principle, to tell in which process a pair of photons is generated unless polarizations are measured. Therefore, polarization-entangled photons can be generated inherently on the chip without the need of any extra component.

Polarization entanglement can also be produced by the type-II process on the same chip. Following the same formalism, the two-photon state of the type-II process can be explicitly written as

$$|\psi'\rangle = \frac{1}{\sqrt{2}} \iint d\omega_1 d\omega_2 [\Phi_{HV}(\omega_1,\omega_2)|H\omega_1, V\omega_2\rangle + \Phi_{VH}(\omega_1,\omega_2)|V\omega_1, H\omega_2\rangle]. \quad (2)$$

For maximal entanglement, it requires $\Phi_{HV}(\omega_1,\omega_2) = \Phi_{VH}(\omega_1,\omega_2)$. This is not satisfied for the waveguide being tested. However, due to the lack of material birefringence and thus very small temporal walkoff, there exists a significant amount of overlap between $\Phi_{HV}(\omega_1,\omega_2)$ and $\Phi_{VH}(\omega_1,\omega_2)$. The corresponding spectra are shown in Fig. 2(b). As a result, entanglement exists even without any compensation and bandpass filtering.

Photons in a pair need to be spatially separated. In this work, we used a 50:50 beam splitter to separate photons non-deterministically followed by postselection. However, paired photons can also be separated deterministically by a dichroic mirror or an integrated dichroic splitter as was done in [20]. For an ideal dichroic mirror that has a splitting wavelength at the degenerate point, the degree of entanglement is identical to that using a 50:50 beam splitter.

III. SAMPLE DESCRIPTION AND EXPERIMENTAL DETAILS

As a proof of principle demonstration, a wafer designed for type-I PM around 1550 nm [25] is used to demonstrate this entangled photon source. Waveguides of this structure are lithographically tuned in order to satisfy concurrent PM of type-0 and type-I processes, with an etch depth of 6.5 μm and multiple ridge widths centered at 1.5 μm with a step size of 20 nm. A scanning electron microscope image of a waveguide is shown in Fig. 1(b). Numerical simulations predict that concurrent PM of the two types can be achieved at a wavelength around 1.63 μm with a ridge width of $\sim$1.5 μm. Note that redesigning the epitaxial structure can shift the center wavelength to 1550 nm [23]. The sample being tested had a length of 1.05 mm.

In order to select the waveguide that has the best alignment of its PM wavelengths, second-harmonic generation (SHG) for both type-0 and type-I processes was tested. The experiment was carried out on a standard end-fire coupling setup by pumping the waveguides with an optical parametric oscillator (OPO) pumped by a femtosecond pulsed Ti:sapphire laser. The normalized SHG tuning curves of the waveguide being tested are shown in Fig. 3(a). According to Fig. 3(a), PM wavelengths of both types are near 1640 nm, the longest achievable wavelength of the OPO used. Due to the large bandwidth of the pump pulse, the exact PM wavelengths could not be accurately identified. Spontaneous parametric down-conversion was then carried out by pumping the waveguides with a cw Ti:sapphire laser where the dependence of a single-photon count rate on the pump wavelength was measured. This allowed us to locate the waveguide that has the best overlap in PM wavelengths among all tested waveguides. The results of the waveguide selected, shown in Fig. 3(b), indicate that the PM wavelengths of both types are 816.7 ± 0.3 nm. The uncertainty in the PM wavelength measurement was due to the pump power fluctuation in the waveguide because of Fabry-Pérot resonances, which could not be resolved with the instrumentation available.

To generate polarization-entangled photons via concurrent type-0 and type-I processes, the TM-polarized pump beam from a cw Ti:sapphire laser was coupled into the waveguide using a 100× objective lens (with a numerical aperture of 0.90), with a power of 1.13 mW before the lens. Photon pairs generated were collected by a 40× objective lens at the output facet and passed through long pass filters to eliminate the pump. After their separation using a 50:50 beam splitter,

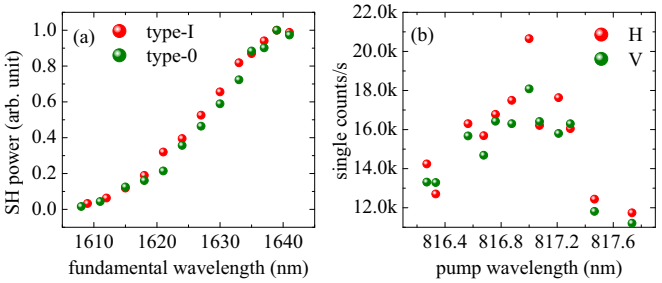

FIG. 3. (Color online) (a) Normalized SHG tuning curves for type-0 and type-I processes of the waveguide under test and (b) the single counts versus pump wavelength for the H- and V-polarized photons generated from type-I and type-0 processes, respectively, with a fixed pump power. For the tuning curves shown in (a), the maximal wavelength is limited to the longest available wavelength of the pump OPO used in the experiment ($\sim$1640 nm).

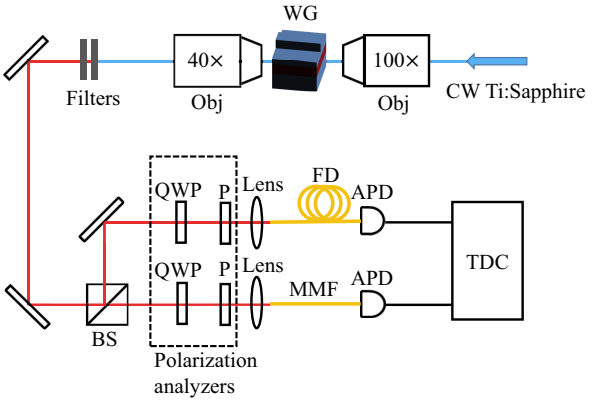

FIG. 4. (Color online) Schematic of the experimental setup for polarization-entangled photon generation. The waveguide was pumped by a cw Ti:sapphire laser in an end fire setup, with a 100× input objective lens and a 40× output objective. Paired photons generated were separated by a 50:50 beam splitter and passed though a pair of polarization analyzers consisting of a QWP and a polarizer. A pair of multimode fiber coupled InGaAs single-photon detectors was used to detect the photons and the coincidence counting histograms were recorded by a TDC. The following denotations were used: Obj, objective; WG, waveguide; BS, beam splitter; QWP, quarter-wave plate; P, polarizer; MMF, multimode fiber; FD, fiber delay; APD, InGaAs avalanche photodiode; and TDC, time-to-digital converter.

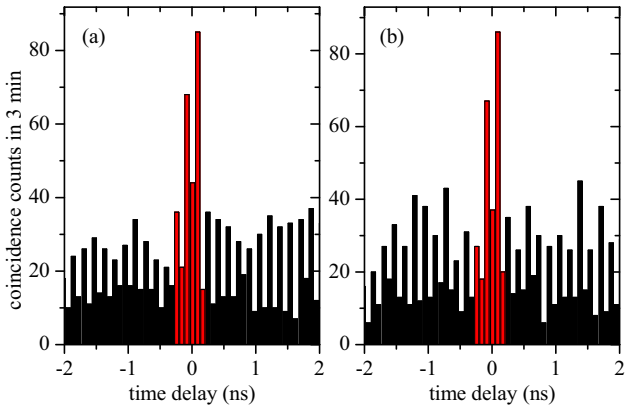

FIG. 5. (Color online) Coincidence histograms of photon pairs in the (a) HH and (b) VV bases for an integration time of 3 min. The red bars around the peaks represent the counts in the coincidence window of ∼0.5 ns.

the signal and idler photons were collected into multimode fibers and detected by two InGaAs single-photon detectors. The signal arm detector (ID220, ID Quantique) operated in a free-running mode and provided 20% efficiency at 1550 nm. The idler detector (ID210, ID Quantique) operated in a gated mode and provided 25% at 1550 nm. It was externally triggered by the detection events of the first detector. An optical delay was added before the second detector to compensate for the electronic delay between the two detectors. Both detectors had a dead time of 20 μs. The coincidence counts were recorded with the help of a time-to-digital converter (TDC) circuitry. At the degenerate wavelength of ∼1635 nm, the detection efficiencies were around 4% and 5%, respectively. A pair of quarter-wave plates (QWPs) and polarizers were used to measure the polarizations of the photon pairs. The schematic of the experimental setup is illustrated in Fig. 4. Considering the transmission coefficients of the output objective lens (90%), long pass filters (70%), the beam splitter (43%), QWPs and polarizers (75%), and fiber collection efficiencies in each path (53% and 34%), the overall collection efficiency of photon pairs with respect to the position right after the waveguide output facet was found to be ∼1.5%.

IV. RESULTS AND DISCUSSION

Typical coincidence histograms are given in Fig. 5(a) for two H-polarized photons and in Fig. 5(b) for two V-polarized photons for a pump wavelength of 816.76 nm and an integration time of 3 min. The coincidence peaks indicate that photon pairs were generated via both type-I and type-0 processes. The high level of accidental counts is due to detector dark counts and broken photon pairs due to waveguide losses as well as limited collection (1.5%) and detection (0.2%) efficiencies. By blocking the idler arm, we found that the dark counts of the second detector consists of 83% of the total accidental counts. Thus we can expect a much higher coincidence-to-accidental ratio by redesigning a sample that generates photon pairs in region where the detectors are more efficient (e.g., at 1550 nm).

The net coincidence count rates for both type-0 and type-I processes are around 0.7 Hz, after subtracting the accidental counts. Taking into account the signal arm detector's dead time, the single count rate (16 kHz), and the overall collection and detection efficiencies, we estimate the photon pair generation rates after the waveguide to be 3.4×10^4 pairs/s. The input objective lens has a transmission of 70% and the coupling efficiency into the pump Bragg mode is estimated to be 6%, resulting in an internal pump power of 47.3 μ W right after the input facet. Therefore, the photon pair production rates are both around 7.3×10^5 (pairs/s)/mW with respect to the internal pump power and external photon pairs or, equivalently, 1.8×10^{-10} pairs/pump photon. The fact that both processes have roughly the same generation rates, as opposed to the type-I process being more efficient than the type-0 process according to theoretical calculation, could be because the TM mode has a smaller loss than that of the TE mode in this type of deeply etched waveguide. We confirmed this by measuring the losses using the Fabry-Pérot method and found the losses to be 4.3 and 2.5 cm^{-1} for TE and TM modes, respectively. It could also be because the pump wavelength is slightly detuned from the degenerate PM wavelength of the more efficient process, as the two processes may not have exactly identical PM wavelengths.

Quantum state tomography measurements were then subsequently performed by projecting the paired photons into 16 polarization combinations and the density matrix was reconstructed using the maximal-likelihood method [26,27]. The net density matrix ρ of the output two-photon state, given by Fig. 6, is found to have a concurrence [28] of 0.85 ± 0.07. The maximum fidelity with a maximally entangled state $|\Phi\rangle = [|H,H\rangle + \exp(i\phi)|V,V\rangle]/\sqrt{2}$, defined by $F = \max_\phi \langle\Phi|\rho|\Phi\rangle$, is 0.89 with a corresponding phase angle $\phi = 40^\circ$. The nonzero phase ϕ is because of the

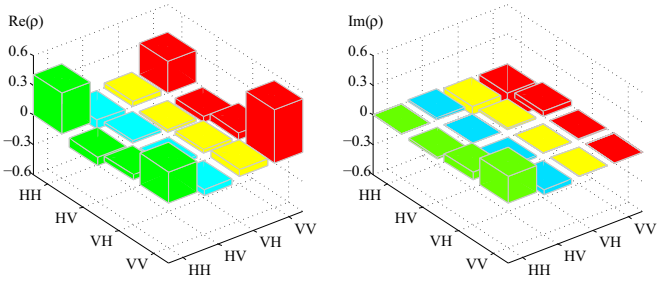

FIG. 6. (Color online) Real and imaginary parts of the reconstructed density matrix of the output two-photon state via concurrent type-0 and type-I processes.

slightly dissimilar degenerate PM wavelengths of the two processes. Theoretical calculation according to Eq. (1) shows that this phase value is due to the type-I PM wavelength being ∼0.02 nm shorter than that of the type-0 process. The imperfection of the entanglement could be mainly because the pump wavelength is not optimal, causing extra spectral distinguishability between the two processes. This can be improved by using a tunable diode laser that has a fine spectral tunability. In addition, the mechanical drift of the characterization setup could result in an increase of mixture and a decrease of entanglement for measurements longer than a few minutes.

The fact that a slightly different PM wavelengths causes one of the processes to take place below its maximal generation rate can be used to balance the generation rates of the two processes and therefore increase the degree of entanglement. Although engineering efforts can be made to achieve almost identical efficiencies, in reality, there may still be differences, especially with the existence of polarization-dependent losses. In such a case, the waveguide ridge width can be lithographically tuned such that the stronger process has a shorter PM wavelength, while the pump wavelength should be tuned to the degenerate PM wavelength of the weaker process.

To illustrate this point, we consider an example where the type-I process is twice as efficient as the type-0 process, i.e., $\eta_I = 2\eta_0$. In the case where the two PM wavelengths are identical, the theoretical fidelity to a maximally entangled state is 0.96 and the concurrence is 0.93. The degree of entanglement can be increased to near maximum by tuning the ridge width such that the PM wavelength of the type-I process is 0.55 nm below that of the type-0 process. The corresponding tuning curves of the two processes weighted by their efficiencies are shown in Fig. 7(a). The pump wavelength, marked by the white line, is fixed at the degenerate PM wavelength of the type-0 process. In this case, the spectra, given by Fig. 7(b), show almost the same amplitude, indicating that the two processes have the same spectral brightness near the degenerate wavelength. By utilizing a weak spectral filtering with a bandwidth of 80 nm, the calculated fidelity and concurrence are increased to 0.997 and 0.995, respectively, with $\phi = 34^\circ$, indicating the generation of maximally entangled photons. Without bandpass filtering, the maximum fidelity and concurrence can still reach 0.99 and 0.97, respectively, with a phase $\phi = 14^\circ$, when the type-I PM wavelength is 0.36 nm below that of the type-0 process. In addition, this

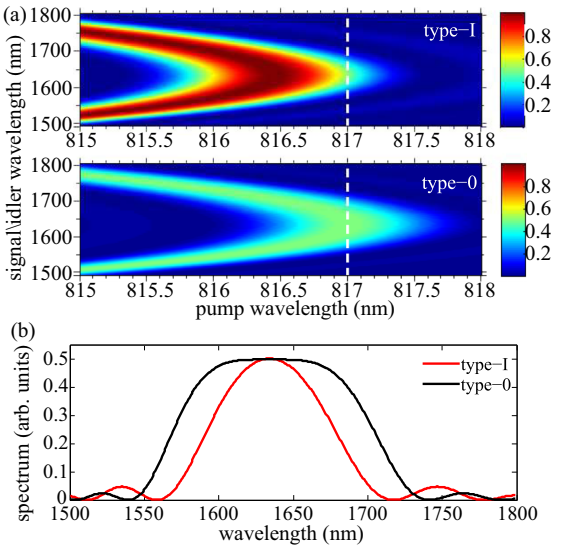

FIG. 7. (Color online) (a) Turning curves of the type-I (top) and type-0 (bottom) processes weighted by the corresponding efficiencies. The white dashed lines represent the pump wavelength. (b) Corresponding spectra of the down-converted photons.

tuning approach could be used to generate nonmaximally entangled states $[|H,H\rangle + r\exp(i\phi)|V,V\rangle]/\sqrt{1+r^2}$ with a tunable value of r, which offers significant advantages over maximally entangled states in some applications such as closing the detection loophole in quantum nonlocality tests [29].

Finally, we show the generation of cross-polarized polarization-entangled photons on the same chip via the type-II process. For a TE-polarized pump at 812.92 nm, which is only less than 4 nm below those of type-0 and type-I processes, the output state, again without any compensation and bandpass filtering, shows a concurrence of 0.55 ± 0.08 and a fidelity of 0.74 to the maximally entangled state $[|H,V\rangle + \exp(i\phi)|V,H\rangle]/\sqrt{2}$. The degree of entanglement is comparable with that obtained in [20]. The reconstructed density matrix is given by Fig. 8. The utility of this device becomes most apparent when one considers its capability of having all three types of PM simultaneously achieved at the same wavelength via the tuning of the epitaxial structure combined with ridge width control [30]. The unique ability to achieve this monolithically allows the generation of

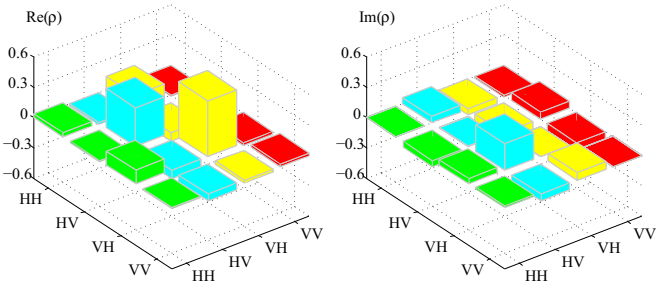

FIG. 8. (Color online) Real (left) and imaginary (right) parts of the reconstructed density matrix of the output two-photon state generated via the type-II process.

both copolarized and cross-polarized polarization-entangled photons on the same chip at the same pump wavelength, by simply selecting the pump polarization. Nevertheless, a difference of a few nanometers in the PM wavelength can be covered by a femtosecond pump laser.

V. CONCLUSION

We have demonstrated how the waveguiding physics associated with BRWs can be used to simultaneously produce two polarization-entangled photon sources using alternative approaches in a single self-contained room-temperature semiconductor chip. Direct generation of polarization-entangled photons from a monolithic compound semiconductor chip via concurrent type-0 and type-I SPDC processes has been characterized. Simultaneous PM of the two processes was achieved using simple lithographic control on the ridge width of BRWs. Without the need of off-chip compensation, an interferometer, and a bandpass filter, the degree of entanglement is among the highest in previous demonstrations from monolithic III–V and Si chips. In addition, the same device can also directly generate polarization entanglement via the type-II process, with a pump wavelength only 4 nm shorter.

Further improvement of the device performance relies largely on improved fabrications. By reducing the waveguide losses, the generation rates can potentially be increased by more than two orders of magnitudes, as predicted in [24] for lossless waveguides. In addition, the degree of entanglement can be increased by fine-tuning the ridge width via more precise fabrications, as we have shown that the entanglement can be nearly maximal in the ideal case [23]. The degree of entanglement can also be easily increased by bandpass filtering [31].

Note that previous work on ferroelectric waveguides also studied the diversity of multiple PM processes to generate quantum states of particular properties, such as using two quasi-phase-matching gratings to generate polarization-entangled photons [32,33] and using different spatial modes to achieve mode entanglement [34]. While they are fundamentally important, realizing such effects in monolithic fashions, especially on III–V semiconductor platforms as in this work, offers many possibilities for practical optical quantum information processing.

ACKNOWLEDGMENTS

The authors would like to acknowledge R. Marchildon, G. Egorov, F. Xu, E. Zhu, and Z. Tang for helpful discussions. This work was supported by Natural Sciences and Engineering Research Council of Canada.

[1] T. D. Ladd, F. Jelezko, R. Laflamme, Y. Nakamura, C. Monroe, and J. L. O'Brien, Quantum computers, Nature (London) **464**, 45 (2010).

[2] N. Gisin, G. Ribordy, W. Tittel, and H. Zbinden, Quantum cryptography, Rev. Mod. Phys. **74**, 145 (2002).

[3] A. Christ, A. Fedrizzi, H. Hübel, T. Jennewein, and C. Silberhorn, Parametric Down-Conversion, Exp. Methods Phys. Sci. **45**, 351 (2013).

[4] J. L. O'Brien, A. Furusawa, and J. Vučković, Photonic quantum technologies, Nat. Photon. **3**, 687 (2009).

[5] A. Gaggero, S. Jahanmiri Nejad, F. Marsili, F. Mattioli, R. Leoni, D. Bitauld, D. Sahin, G. J. Hamhuis, R. Nötzel, R. Sanjines, and A. Fiore, Nanowire superconducting single-photon detectors on GaAs for integrated quantum photonic applications, Appl. Phys. Lett. **97**, 151108 (2010).

[6] J. W. Silverstone, D. Bonneau, K. Ohira, N. Suzuki, H. Yoshida, N. Iizuka, M. Ezaki, C. M. Natarajan, M. G. Tanner, R. H. Hadfield, V. Zwiller, G. D. Marshall, J. G. Rarity, J. L. O'Brien, and M. G. Thompson, On-chip quantum interference between silicon photon-pair sources, Nat. Photon. **8**, 104 (2014)

[7] H. Jin, F. M. Liu, P. Xu, J. L. Xia, M. L. Zhong, Y. Yuan, J. W. Zhou, Y. X. Gong, W. Wang, and S. N. Zhu, On-chip generation and manipulation of entangled photons based on reconfigurable lithium-niobate waveguide circuits, Phys. Rev. Lett. **113**, 103601 (2014).

[8] T. Suhara, Generation of quantum-entangled twin photons by waveguide nonlinear-optic devices, Laser Photon. Rev. **3**, 370 (2009).

[9] S. V. Zhukovsky, D. Kang, P. Abolghasem, L. G. Helt, J. E. Sipe, and A. S. Helmy, Proposal for on-chip generation and control of photon hyperentanglement, Opt. Lett. **36**, 3548 (2011).

[10] D. Kang, L. G. Helt, S. V. Zhukovsky, J. P. Torres, J. E. Sipe, and A. S. Helmy, Hyperentangled photon sources in semiconductor waveguides, Phys. Rev. A **89**, 023833 (2014).

[11] P. Abolghasem, M. Hendrych, X. Shi, J. P. Torres, and A. S. Helmy, Bandwidth control of paired photons generated in monolithic Bragg reflection waveguides, Opt. Lett. **34**, 2000 (2009).

[12] A. Valencia, G. Scarcelli, and Y. H. Shih, Distant clock synchronization using entangled photon pairs, Appl. Phys. Lett. **85**, 2655 (2004).

[13] S. Lloyd, Enhanced sensitivity of photodetection via quantum illumination, Science **321**, 1463 (2008).

[14] S. Sauge, M. Swillo, S. Alber-Seifried, G. B. Xavier, J. Waldeback, M. Tengner, D. Ljunggren, and A. Karlsson, Narrowband polarization-entangled photon pairs distributed over a WDM link for qubit networks, Opt. Express **15**, 6926 (2007).

[15] F. Kaiser, A. Issautier, L. A. Ngah, O. Dănilă, H. Herrmann, W. Sohler, A. Martin, and S. Tanzilli, High-quality polarization entanglement state preparation and manipulation in standard telecommunication channels, New J. Phys. **14**, 085015 (2012).

[16] S. Arahira and H. Murai, Nearly degenerate wavelength-multiplexed polarization entanglement by cascaded optical nonlinearities in a PPLN ridge waveguide device, Opt. Express **21**, 7841 (2013).

[17] N. Matsuda, H. L. Jeannic, H. Fukuda, T. Tsuchizawa, W. J. Munro, K. Shimizu, K. Yamada, Y. Tokura, and H. Takesue, A monolithically integrated polarization entangled photon pair source on a silicon chip, Sci. Rep. **2**, 817 (2012).

[18] L. Olislager, J. Safioui, S. Clemmen, K. P. Huy, W. Bogaerts, R. Baets, P. Emplit, and S. Massar, Silicon-on-insulator

integrated source of polarization-entangled photons, Opt. Lett. **38**, 1960 (2013).

[19] A. Orieux, A. Eckstein, A. Lemaître, P. Filloux, I. Favero, G. Leo, T. Coudreau, A. Keller, P. Milman, and S. Ducci, Direct Bell states generation on a III-V semiconductor chip at room temperature, Phys. Rev. Lett. **110**, 160502 (2013).

[20] R. T. Horn, P. Kolenderski, D. Kang, P. Abolghasem, C. Scarcella, A. D. Frera, A. Tosi, L. G. Helt, S. V. Zhukovsky, J. E. Sipe, G. Weihs, A. S. Helmy, and T. Jennewein, Inherent polarization entanglement generated from a monolithic semiconductor chip, Sci. Rep. **3**, 2314 (2013).

[21] B. J. Bijlani, P. Abolghasem, and A. S. Helmy, Semiconductor optical parametric generators in isotropic semiconductor diode lasers, Appl. Phys. Lett. **103**, 091103 (2013).

[22] F. Boitier, A. Orieux, C. Autebert, A. Lemaitre, E. Galopin, C. Manquest, C. Sirtori, I. Favero, G. Leo, and S. Ducci, Electrically injected photon-pair source at room temperature, Phys. Rev. Lett. **112**, 183901 (2014).

[23] D. Kang and A. S. Helmy, Generation of polarization entangled photons using concurrent type-I and type-0 processes in AlGaAs ridge waveguides, Opt. Lett. **37**, 1481 (2012).

[24] S. V. Zhukovsky, L. G. Helt, P. Abolghasem, D. Kang, J. E. Sipe, and A. S. Helmy, Bragg reflection waveguides as integrated sources of entangled photon pairs, J. Opt. Soc. Am. B **29**, 2516 (2012).

[25] P. Abolghasem, J. B. Han, B. J. Bijlani, and A. S. Helmy, Type-0 second order nonlinear interaction in monolithic waveguides of isotropic semiconductors, Opt. Express **18**, 12861 (2010).

[26] D. F. V. James, P. G. Kwiat, W. J. Munro, and A. G. White, Measurement of qubits, Phys. Rev. A **64**, 052312 (2001).

[27] The density-matrix reconstruction was performed using the program provided by the Kwiat Quantum Information Group http://research.physics.illinois.edu/QI/Photonics/tomography/

[28] W. K. Wootters, Entanglement of formation of an arbitrary state of two qubits, Phys. Rev. Lett. **80**, 2245 (1998).

[29] B. G. Christensen, K. T. McCusker, J. B. Altepeter, B. Calkins, T. Gerrits, A. E. Lita, A. Miller, L. K. Shalm, Y. Zhang, S. W. Nam, N. Brunner, C. C. W. Lim, N. Gisin, and P. G. Kwiat, Detection-Loophole-Free test of quantum nonlocality, and applications, Phys. Rev. Lett. **111**, 130406 (2013).

[30] S. V. Zhukovsky, L. G. Helt, D. Kang, P. Abolghasem, A. S. Helmy, and J. E. Sipe, Analytical description of photonic waveguides with multilayer claddings: Towards on-chip generation of entangled photons and Bell states, Opt. Commun. **301**, 127 (2013).

[31] In a separate experiment, we have demonstrated a concurrence of 0.98 via the type-II process in a similar waveguide with bandpass filtering only.

[32] H. Herrmann, X. Yang, A. Thomas, A. Poppe, W. Sohler, and C. Silberhorn, Post-selection free, integrated optical source of non-degenerate, polarization entangled photon pairs, Opt. Express **21**, 27981 (2013).

[33] Y. X. Gong, Z. D. Xie, P. Xu, X. Q. Yu, P. Xue, and S. N. Zhu, Compact source of narrow-band counterpropagating polarization-entangled photon pairs using a single dual-periodically-poled crystal, Phy. Rev. A **84**, 053825 (2011).

[34] P. J. Mosley, A. Christ, A. Eckstein, and C. Silberhorn, Direct measurement of the spatial-spectral structure of waveguided parametric down-conversion, Phys. Rev. Lett. **103**, 233901 (2009).